Structure and magnetic properties of amorphous Fe_xSn_{1-x} alloys

B. Rodmacq, M. Piecuch, Chr. Janot, G. Marchal, and Ph. Mangin
Laboratoire de Physique du Solide, L. A. au Centre National de la Recherche Scientifique No. 155, Faculte des Sciences, C. O. 140, 54037 Nancy, Cedex, France
(Received 19 July 1979)

Amorphous films of Fe_xSn_{1-x} have been prepared by vapor quenching over a wide range of composition ($0.3 < x < 0.8$). Interference functions have been obtained from electron diffraction. Local magnetic properties have been deduced from Mössbauer-spectroscopy data and compared to bulk magnetization which vanishes at a critical composition $x_{cr} \simeq 0.35$. Down to $x = 0.45$, the alloys are ferromagnets with a mixture of magnetic and nonmagnetic iron atoms. Hyperfine field distribution on magnetic iron atoms is due to chemical disorder rather than structure effects. Nonmagnetic iron atoms and tin atoms have been found to experience a weak dipolar or a transferred magnetic field, respectively. The temperature dependence of the hyperfine field in iron-rich alloys ($x > 0.53$) is consistent with predictions of a collective excitation model at low temperature and with a mean-field theory in an intermediate temperature range. A value of the relative distribution width of the exchange integral $\Delta J/J \simeq 0.4$ has been calculated.

I. INTRODUCTION

Amorphous materials have been extensively studied for the last few years. Structural investigations, especially using diffraction methods,[1,2] have shown that short-range order (SRO) along with long-range disorder (LRD) is typical of these materials. Amorphous metals or amorphous metallic alloys have been mostly described in terms of a dense-random-packing-of-hard-spheres model (DRPHS).[1] For both basic science and technical applications, it is of the greatest importance to correlate amorphous structure and the properties of these new species of material. Mostly because of their being soft ferromagnets, a number of amorphous alloys have been considered of interest from the point of view of their magnetic properties. Among them, the Fe_xSn_{1-x} amorphous system is an attractive one. First its electrical-resistivity behavior is typical of a metal whatever the composition[3,4] ($0.3 < x < 0.8$). It is worth noting that the brother amorphous systems Fe_xSi_{1-x} (Ref. 5) and Fe_xGe_{1-x} (Ref. 6) are stable at room temperature over wider compositional ranges (down to $x = 0$) but exhibit a metal $\rightarrow$ semiconductor transition near $x \simeq 0.2$. On the other hand, there is a number of crystalline equilibrium Fe-Sn phases whose structure and magnetic properties are both fairly well known[7] and worth being compared to those of the amorphous alloys (Fe_3Sn, Fe_5Sn_3, and Fe_3Sn_2 are ferromagnets and FeSn and $FeSn_2$ are antiferromagnetic).

In previous papers, we have published data on some physical properties of the Fe_xSn_{1-x} amorphous alloys: resistivity measurements and conductivity model,[4,8] bulk magnetization,[9] and preliminary Mössbauer investigation on the ^{57}Fe isotope.[10,11] The present paper will be mainly devoted to structural studies and detailed description of the magnetic order through the composition and temperature dependences of the hyperfine magnetic field as measured on ^{57}Fe and ^{119}Sn isotopes.

II. EXPERIMENTAL PROCEDURES

A. Sample preparation

As extensively described elsewhere[2-5,9,12] the samples have been obtained by atomic deposition on cooled substrates of tin and iron evaporated from independently regulated electron-gun crucibles. The evaporation rates were controlled by quartz monitoring systems. Thanks to ultra-high-vacuum conditions the pressure was kept less than 2×10^{-8} Torr during the evaporation. The residual atmosphere, as given by quadrupolar mass spectrometer analysis, was found to be mainly made of H_2 (3×10^{-10} Torr), N_2 (1.3×10^{-10} Torr), CO_2 (6×10^{-10} Torr), and H_2O (3×10^{-9} Torr). Thus the sample contamination was less than 1%. The substrates were either carbon-coated microscope grids for diffraction studies or Kapton films for Mössbauer spectroscopy, the thickness of the corresponding amorphous Fe_xSn_{1-x} films being 200–400 Å and 1–2 μm, respectively. Alloys composition was deduced from the indications of the quartz monitoring systems and ascertained by atomic-absorption spectrometry; thus the x value can be considered as known with an error less than 0.01. The samples, warmed up to room temperature, were taken out of the vacuum chamber for subsequent physical studies.

B. Mössbauer spectrometry

The Mössbauer data were collected from a constant-acceleration symmetrical-mode spectrometer, with $^{57}Co^*$-Rh and $Ba^{119}SnO_3$ sources. Hyperfine parameters were measured from liquid-helium temperature up to about 600 K. Alternatively, an external magnetic field ($\leq$60 kG) was applied to the specimens.

C. Diffraction study

Following a method described elsewhere[2] the interference functions $J(K)$ were obtained from diffraction investigation using a classical 100-kV electron microscope. Electron diffraction is more suitable than x-ray or neutron diffraction as far as relatively thin films are concerned.

Unfortunately, inelastic scattering results in quite a large background and a dramatic uncertainty in the diffracted absolute intensity. Thus, it is not worth trying to Fourier transform the obtained interference functions $J(K)$ into spatial pair distribution functions $P(r)$, and the $J(K)$ maximum positions along with the relative variation of the diffracted intensity are practically the only meaningful experimental data.

III. SHORT-RANGE ORDER IN THE Fe_xSn_{1-x} AMORPHOUS ALLOYS

A. Partial interferences functions

The diffraction profiles for Fe_xSn_{1-x} amorphous alloys ($0.40 < \times < 0.75$) are shown in Fig. 1, and the positions K_i, K_i' of the main peak are summarized in Table I, along with the ratios K_i/K_1 of these positions relative to the first sharp maximum. The essential features are as follows:

(i) A strong resemblance of the patterns corresponding to the iron-rich alloys with usual interference functions obtained for pure amorphous metals[13,14] or amorphous alloys made of transition metal (TM) and metalloid (Me) near the $TM_{80}Me_{20}$ composition.[15] In particular the ratios K_2/K_1, K_3/K_1, and K_4/K_1 are very close to those of pure amorphous

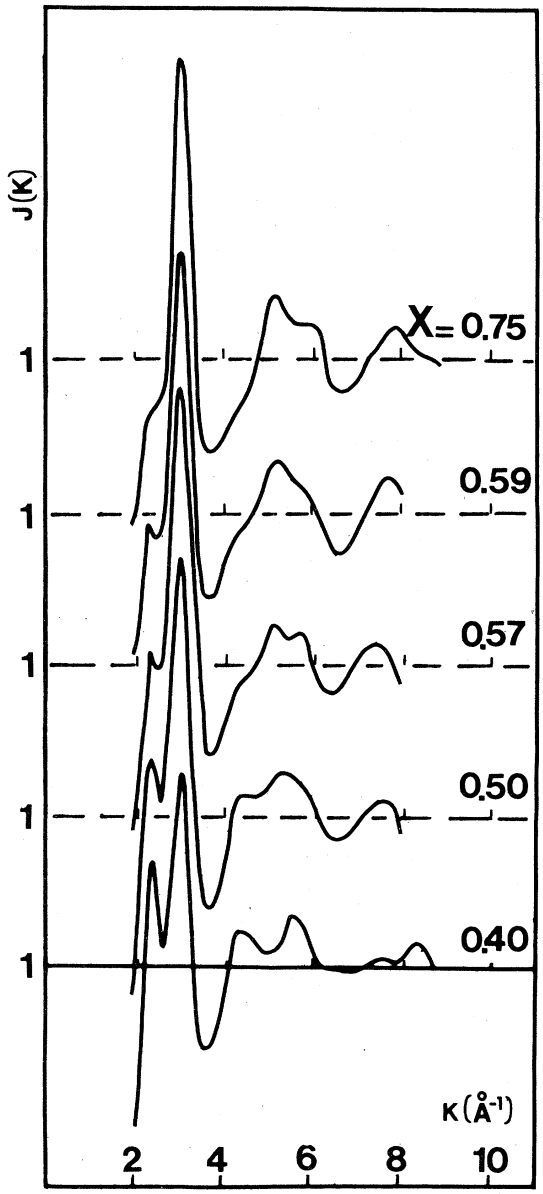

FIG. 1. Interference functions $J(K)$ for amorphous Fe_xSn_{1-x} alloys at different compositions.

TABLE I. Peak positions (in $Å^{-1}$) for the interference functions of Fe_xSn_{1-x} alloys.

x	K_1'	K_1	K_2'	K_2	K_3	K_4	K_2/K_1	K_3/K_1	K_4/K_1	K_2'/K_1'
0.75	2.44	3.03		5.20	5.97	7.86	1.72	1.97	2.59	
0.59	2.33	2.98	4.44	5.15	5.74	7.64	1.73	1.93	2.56	1.90
0.57	2.33	2.96	4.44	5.12	5.65	7.60	1.73	1.91	2.56	1.90
0.50	2.31	2.96	4.43	5.33		7.59	1.80		2.53	1.91
0.40	2.33	3.00	4.34	5.51		7.46	1.84		2.49	1.86

iron, which are 1.73, 2, and 2.60, respectively.[13,14]

(ii) The growth of two extra peaks K_1' and K_2' on both sides of K_1 when the tin concentration increases. At the same time the peaks K_2 and K_3 are progressively fused in only one maximum. Judging from the K_2'/K_1' value, K_2' might be an unresolved structure including $(K_2' - K_3')$ like peaks as in liquid state.

The partial interference functions J_{Fe-Fe}, J_{Fe-Sn}, and J_{Sn-Sn} which describe the contribution of Fe-Fe, Fe-Sn, and Sn-Sn correlations to the total diffraction profile have been calculated in the assumptions that the K_1' peak is due to Sn-Sn correlations and that the three partial functions are independent of composition.

In order to minimize undesirable oscillations a least-squares procedure over all the measured diffraction profile has been used instead of calculating the partial functions as usual from only three experimental patterns. The partial interference functions are shown in Fig. 2. In Table II are reported the corresponding peak positions along with those measured in a Cu_6Sn_5 liquid alloy[16] in pure liquid tin[17] and those calculated for a $Cu_{60}Zr_{40}$ amorphous alloy[18] using a DRPHS model excluding Zr triangles. It is worth comparing these systems because of Cu and Fe, on the one hand, and Zr and Sn, on the other hand, having fairly similar Goldschmidt radii.

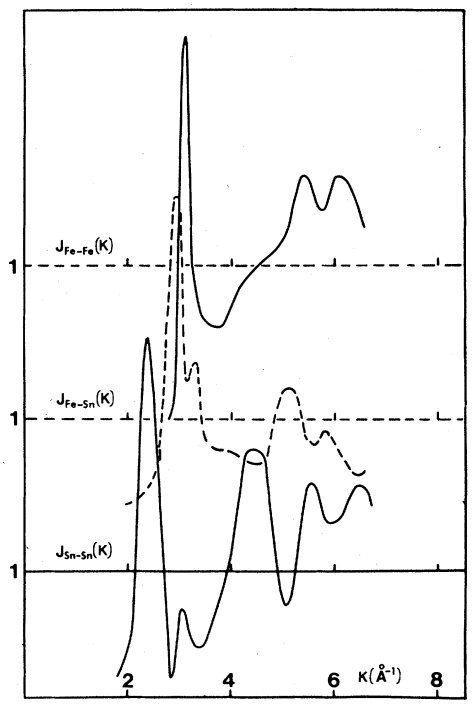

FIG. 2. Partial interference function determined as explained in text.

TABLE II. Comparison between partial interference functions of different disorder systems.

Systems	Partial functions	K_1	K_2	K_3
Amorphous Fe_xSn_{1-x} alloys	J_{Fe-Fe}	3.1	5.4	~6
	J_{Fe-Sn}	2.90	5.1	
	J_{Sn-Sn}	2.30	4.40	~5.5
Liquid Cu_6Sn_5 alloy	J_{Cu-Cu}	2.75	5.22	
	J_{Cu-Sn}	2.87	5.20	
	J_{Sn-Sn}	2.26	4.38	6.78
Liquid Sn	J_{Sn-Sn}	2.24	4.39	6.43
Amorphous $Cu_{60}Zr_{40}$ alloy (calculated)	J_{Cu-Cu}	2.84	4.95	5.87
	J_{Cu-Zr}	1.85	3.12	5.14
	J_{Zr-Zr}	1.74	2.84	4.50

B. Structure of the Fe_xSn_{1-x} amorphous alloys

Metallic amorphous alloys are usually described in terms of a DRPHS model. The conclusions suggested by the data of Table II seem less simple.

(i) The partial functions J_{Sn-Sn} are quite similar in Fe_xSn_{1-x}, liquid Cu_6Sn_5 and liquid pure Sn ($K_1 \sim 2.3$; $K_2 \sim 4.4$) but are different from that expected from hard-sphere packing [see calculated J_{Zr-Zr} ($K_1 \simeq 1.8$; $K_2 \simeq 2.8$) in $Cu_{60}Zr_{40}$]. Thus the tin atoms could be in a liquid-like state as already pointed out.

(ii) The partial functions J_{Fe-Sn} and J_{Cu-Sn} are also similar to each other ($K_1 \sim 2.9$; $K_2 \sim 5.1$) but are far from that of hard-sphere correlation ($K_1 \sim 1.8$; $K_2 \sim 3.1$).

(iii) The partial functions J_{Fe-Fe} and J_{Cu-Cu} have some similarities whatever the system ($K_1 \sim 2.9$; $K_2 \sim 5.2$) and are well interpreted by a hard-sphere-packing model. Moreover, these partial functions are not typically different from those describing the mixed correlation Fe-Sn and Cu-Sn.

Thus we can conclude that the structure of amorphous Fe_xSn_{1-x} alloys is not as close packed as that of a pure amorphous metal. In particular the Sn-Sn and Sn-Fe correlations might suggest a more open partial short-range order perhaps with tin atoms arranged in a liquid-like structure and the smaller iron atoms filling "holes" in this network.

A detailed structural model taking account of some sort of chemical correlation will be proposed in a next paper by comparing the diffraction profiles obtained for Fe_xSn_{1-x} and for brother systems (MnSn, CoSn, NiSn, CuSn) whose study is in progress in our laboratory.

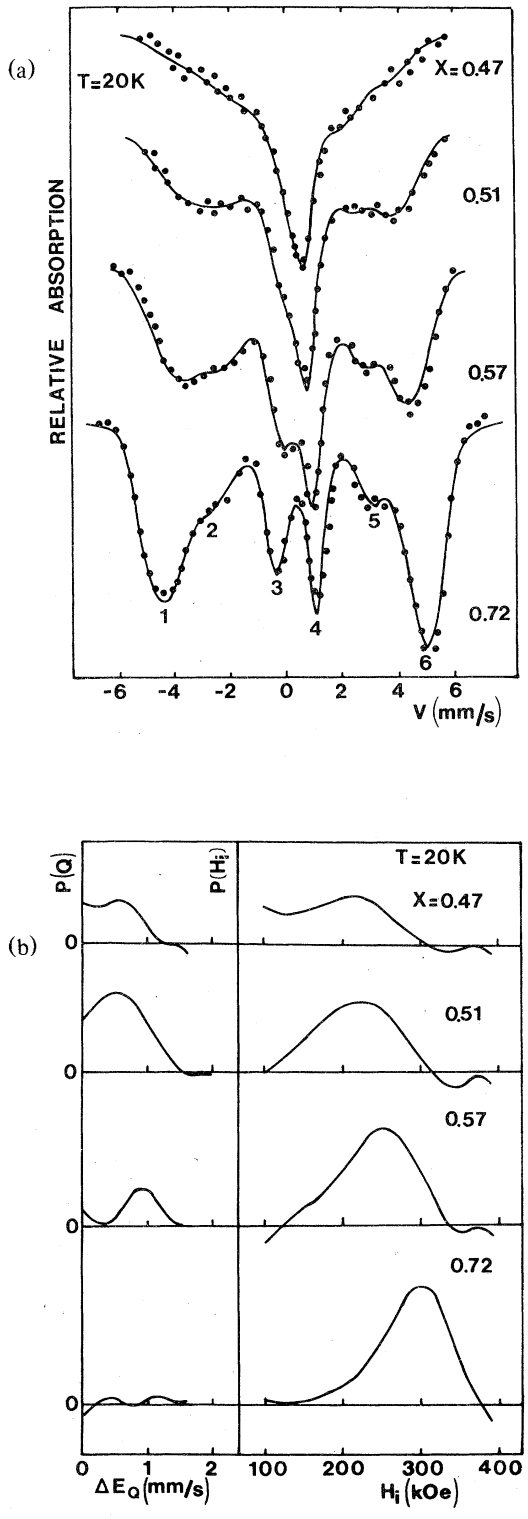

FIG. 3. (a) ^{57}Fe Mössbauer spectra at $T=20$ K for various Fe_xSn_{1-x} amorphous alloys. (b) Hyperfine field distribution $P(H)$ and quadrupolar effect distribution $P(Q)$ corresponding to the spectra of (a).

IV. MÖSSBAUER-SPECTROSCOPY STUDY OF THE MAGNETIC PROPERTIES

A. Experimental results and spectrum analysis

Typical Mössbauer spectra of ^{57}Fe in the amorphous Fe_xSn_{1-x} system are shown in Figs. 3(a) and 4(a).

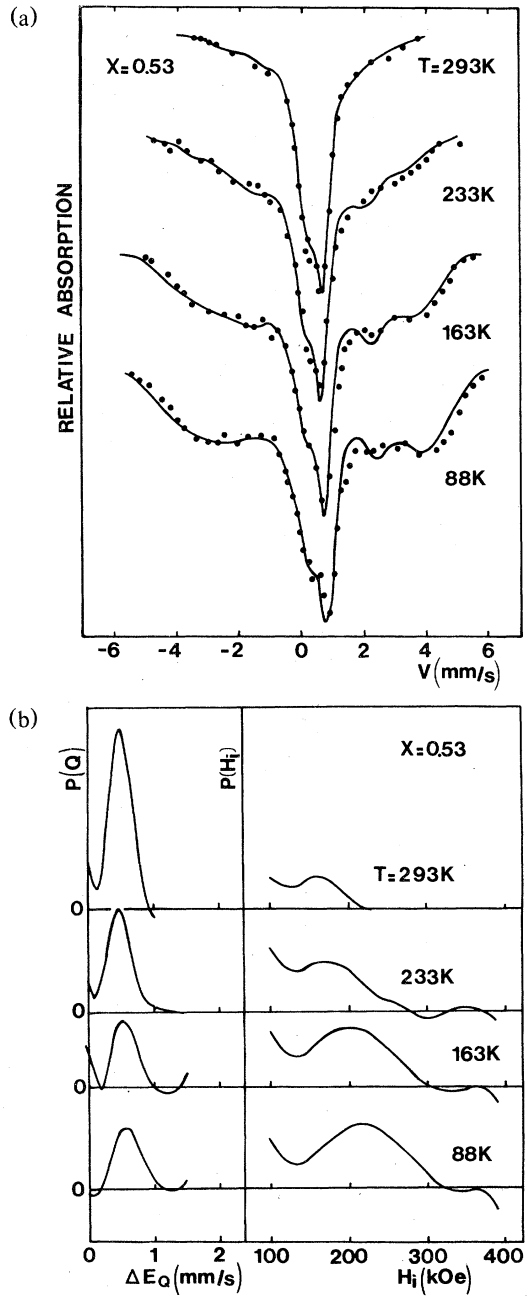

FIG. 4. (a) ^{57}Fe Mössbauer spectra recorded at different temperatures from the $Fe_{0.53}Sn_{0.47}$ alloy. (b) Hyperfine field distribution $P(H)$ and quadrupolar effect distribution $P(Q)$ corresponding to the spectra of (a).

As is usual in disordered systems,[19,20] these Mössbauer spectra have fairly broad peaks, mostly arranged in an asymmetrical sextuplet for alloys of the iron-rich end, in an asymmetrical doublet for alloys of the other side and having both contributions in the intermediate composition. Experiments carried out with an external magnetic field applied to the specimens have shown that the sextuplet component may be ascribed to "magnetic iron atoms" (i.e., having a magnetic moment) and the doublet component to "nonmagnetic iron atoms" (i.e., having no magnetic moment). Warming the alloy or reducing its iron content results in decreasing the relative concentration C_H of magnetic atoms. On the other hand, the amorphous films exhibit uniaxial magnetic anisotropy with the hyperfine field direction almost perpendicular to the film plan ($||$ to the γ rays) as seen from the relative weak intensity of the peaks number 2 and 5 [Fig. 3(a)].

In the particular case of amorphous Fe_xSn_{1-x} alloys, we have explained elsewhere[11] that the asymmetry of the sextuplet component was due to correlation between hyperfine field H_i and isomer shift δ (with respect to metallic iron) according to

$$\delta(\text{mm sec}^{-1}) = 0.838 - 2.54 \times 10^{-3} H_i(\text{kOe}) \ .$$

Thus, the Mössbauer spectra have been analyzed in terms of continuous distributions of hyperfine field $P(H_i)$ and quadrupolar interaction $P(Q)$ using a least-squares calculation as previously explained.[11,19,21] Typical shapes of these distributions are shown in Figs. 3(b) and 4(b). It is worth noting that the width of the $P(H_i)$ curves ($\sim$100 kOe at half maximum) is very large compared to that due to dipolar effects ($\sim$30 kOe) as measured in FeSn crystalline compound and must rather be ascribed to chemical disorder effects.

The numerical values of $P(H_i)$ and $P(Q)$ have been normalized to unity, so that

$$\sum_{\Delta E_Q} P(Q) + \sum_{H_i} P(H_i) = 1$$

and used to calculate the mean hyperfine field in the material

$$\overline{H}_i(x,T) = \sum_{0}^{H_i^{\max}} H_i P(H_i) \ ,$$

whose behavior is expected to be somewhat similar to that of the bulk magnetization. The proportion $C_H(x,T)$ of magnetic iron atoms in the alloy is

$$C_H(x,T) = \sum P(H_i)$$

and the mean quadrupolar interaction for nonmagnetic iron atoms is

$$\overline{\Delta E}_Q(x,T) = \frac{\sum_{0}^{\Delta E_Q^{\max}} \Delta E_Q P(Q)}{\sum P(Q)} \ .$$

These quantities are plotted versus T in Fig. 5 for different alloy compositions. Extrapolating the

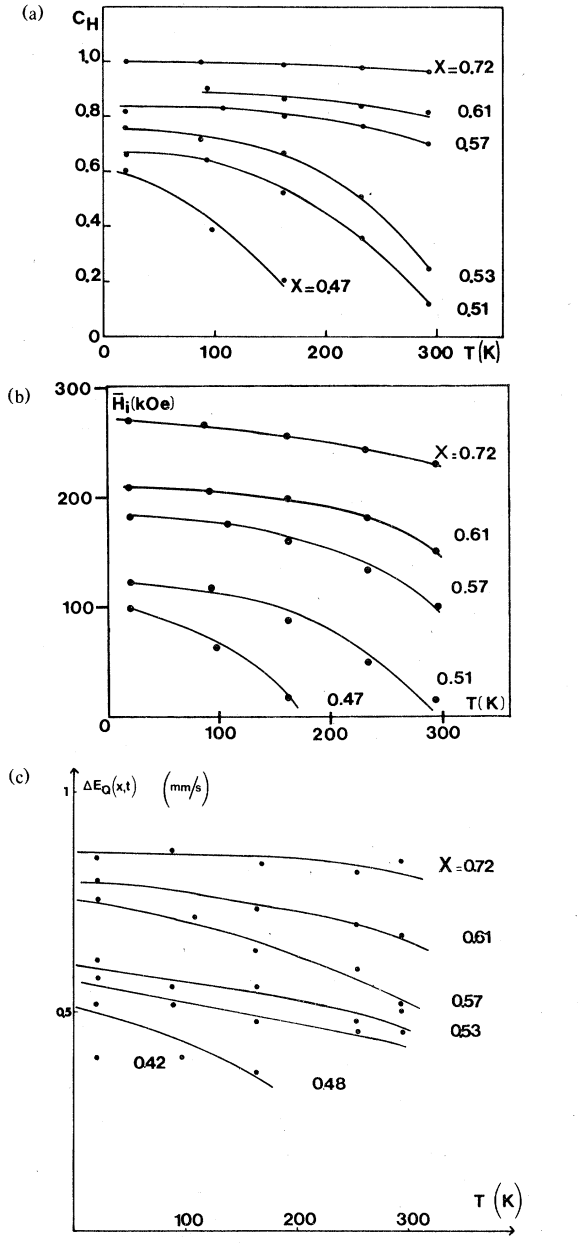

FIG. 5. (a) Temperature and composition dependences of the concentration of magnetic atoms C_H. (b) ΔE_Q of the mean hyperfine field $\overline{H}_i$. (c) ΔE_Q of mean quadrupolar interaction on nonmagnetic atoms.

TABLE III. Mössbauer parameters extrapolated at 0 K for amorphous Fe_xSn_{1-x} alloys.

x	0.72	0.61	0.57	0.53	0.51	0.48	0.42	0.37
$\overline{\Delta E}_Q(x,0)$ (mm sec^{-1})	0.85	0.80	0.76	0.62	0.58	0.56	0.40	0
$\overline{H}_i(x,0)$ (kOe)	272	216	183	166	124	100	59	11
$C_H(x,0)$	100	0.88	0.83	0.76	0.68	0.57	0.40	0.20
T_C (K)	550	420	360	310	300	185	40	25

curves to $C_H(x,T_C)=0$ or $\overline{H}_i(x,T_C)=0$ gives an estimate of the Curie temperature T_C. On the other hand, some kind of "saturation" values $C_H(x,0)$, $\overline{H}_i(x,0)$, and $\overline{\Delta E}_Q(x,0)$ can be obtained by extrapolation to $T=0$. All these data are reported in Table III and are shown in Fig. 6.

Another interesting experimental feature is pictured in Fig. 7 where $\overline{\Delta E}_Q(x,T)$ is plotted versus $\overline{H}_i(x,T)$. Thus the quadrupolar interaction on nonmagnetic iron atoms is a linear function of the mean hyperfine field produced by magnetic iron atoms in the material.

Typical Mössbauer spectra of ^{119}Sn in the amorphous films are shown in Fig. 8. Although somewhat hazardous the analysis of these spectra in terms of hyperfine field distribution has been attempted (Fig. 8); the proportion C_{tH} of tin atoms submitted to a transferred hyperfine field and the mean transferred field $\overline{H}_t$ have been calculated in the assumption that the "low field" part of the distributions $P(H_t)$ actually corresponds to $H_t=0$. The alloy composition dependences of $C_{tH}(x,0)$ and $\overline{H}_t(x,0)$ are shown in Fig. 9 along with the corresponding data for iron atoms $C_H(x,0)$ and $\overline{H}_i(x,0)$. The tin spectra and their $P(H_t)$ distribution are very similar to that observed in Heusler alloys.[22]

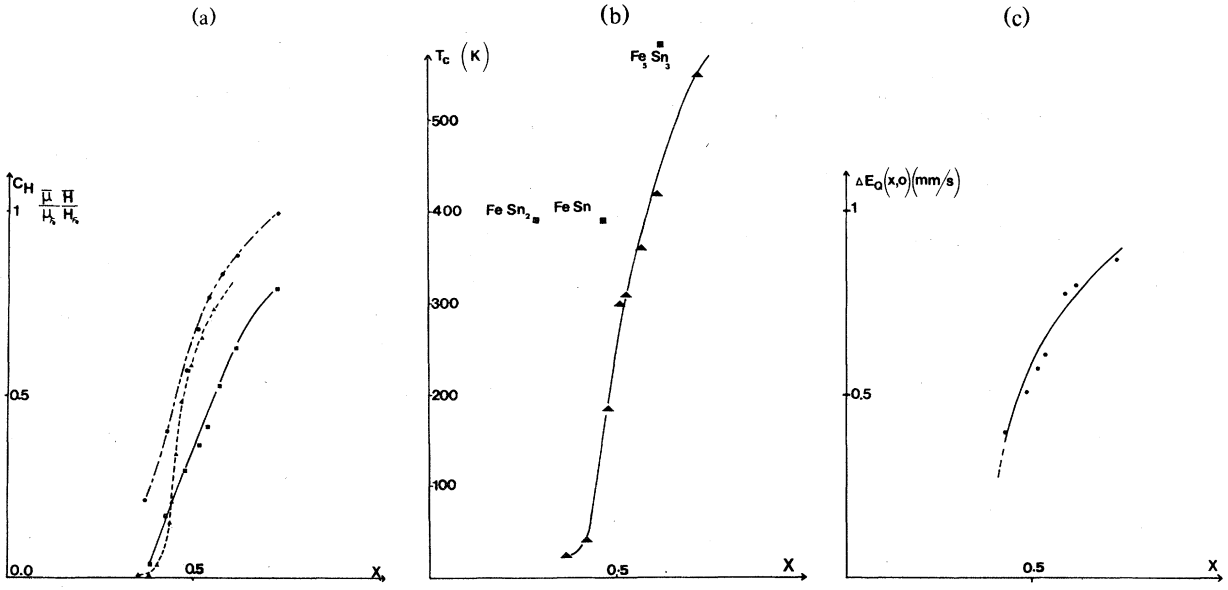

FIG. 6. (a) Zero-temperature concentration of magnetic atoms (●), reduced zero-temperature mean hyperfine field (▲), and reduced mean bulk magnetic moment (■) vs iron concentrations. (b) Curie temperature of amorphous Fe_xSn_{1-x} alloys (▲) and Curie temperature of some crystalline iron-tin compounds (■). (c) Mean quadrupolar effect on nonmagnetic atoms extrapolated to zero temperature vs iron concentration.

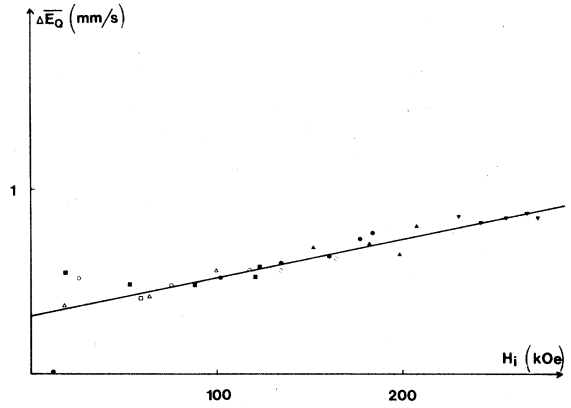

FIG. 7. Mean quadrupolar effect on nonmagnetic atoms vs mean hyperfine field: ▼, $x=0.72$; ▲, $x=0.61$; ●, $x=0.57$; ○, $x=0.53$; ■, $x=0.51$; Δ, $x=0.48$; □, $x=0.42$; *, $x=0.37$.

B. Alloy-composition dependence of the magnetic properties and discussion

It is clear from the curves presented in Figs. 5, 6, and 9 that magnetism ($\overline{H}_i$, $\overline{H}_t$, $\overline{\mu}$, C_H, C_{tH}, and T_C) disappears in the Fe_xSn_{1-x} amorphous alloys when the iron concentration is about 35%. The relative concentration of tin atoms C_{tH} experiencing a transferred field is practically equal to the relative concentration of magnetic iron atoms C_H over almost the whole compositional range. It suggests the existence of some sort of "local magnetic configurations" which are the only ones to contribute to both hyperfine field on ^{57}Fe and transferred field on ^{119}Sn. It suggests also that the transferred magnetism to tin is a short-range effect.

Above the critical iron concentration $x_{cr} \simeq 0.35$, the reduced mean hyperfine field $\overline{H}_i(x,0)/\overline{H}_i(1,0)$ is mostly smaller than the reduced bulk magnetization $\overline{\mu}(x,0)/\mu(1,0)$ [Fig. 6(a)]. It means that these amorphous alloys are ferromagnetic, especially near $x \simeq 0.5$ contrary to the corresponding crystalline compound FeSn which is an antiferromagnet. The magnetic parameters $\overline{H}_i$ and $\overline{\mu}$ of the ferromagnetic crystalline compounds Fe_3Sn, Fe_5Sn_3, and Fe_3Sn_2 are almost the same as those of the corresponding amorphous alloys $Fe_{75}Sn_{25}$, $Fe_{62,5}Sn_{37,5}$, and $Fe_{60}Sn_{40}$, [Fig. 6(a)] which means that the mean hyperfine field and the proportion of magnetic atoms are mainly influenced by chemical disorder. However, the Curie temperatures are significantly lower in amorphous than in crystalline compounds which is probably due to a structural effect on the exchange integral value and distribution [Fig. 6(b)].

So, assuming that the hyperfine field measured on a given iron atom in an iron-tin compound is entirely

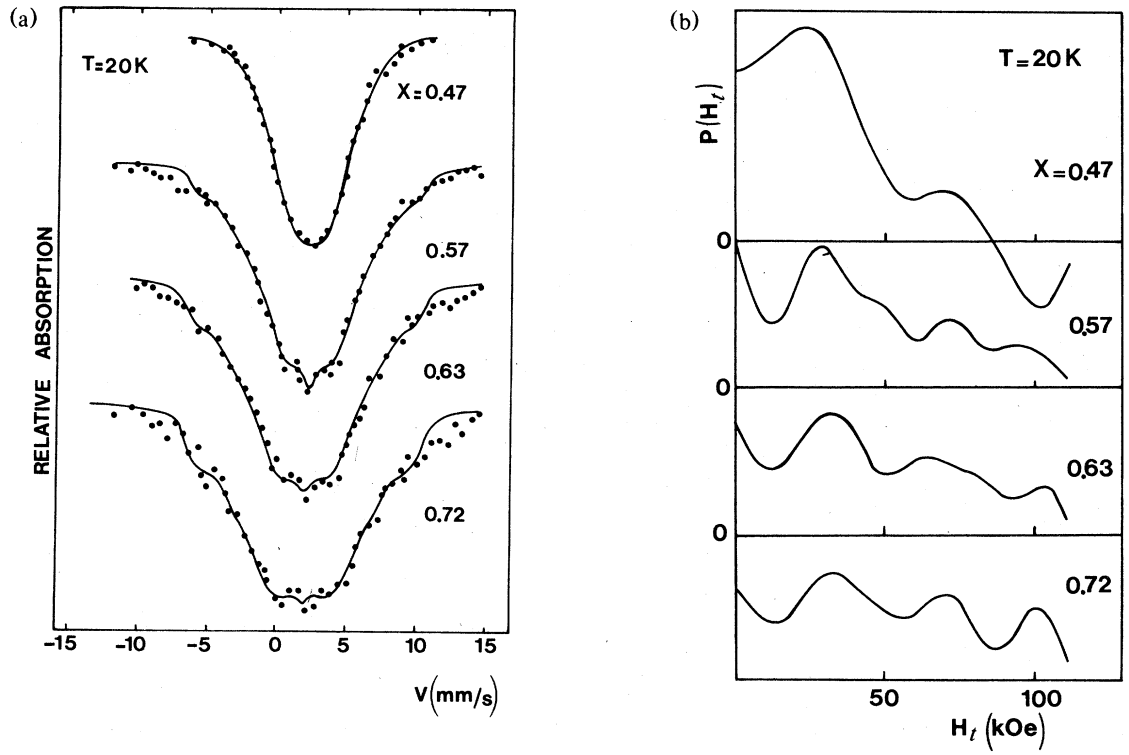

FIG. 8(a). ^{119}Sn Mössbauer spectra at $T=20$ K for Fe_xSn_{1-x} amorphous alloy at different compositions. (b) Hyperfine field distribution for the spectra of (a).

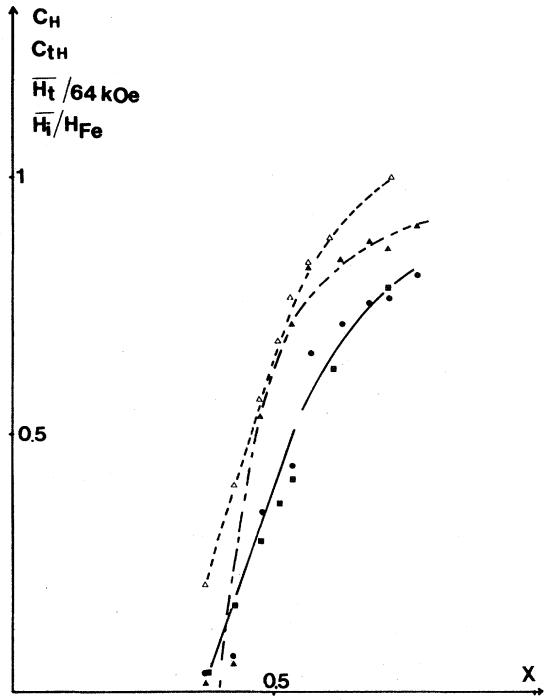

FIG. 9. Concentration of iron magnetic atoms $C_H(\Delta)$, concentration of tin magnetic atoms $C_{tH}(\blacktriangle)$, reduced iron mean hyperfine field (■), and reduced tin mean hyperfine field (●).

determined by the number of its iron-atom nearest neighbors n (Fe), we have used the empirical formula

$$H_i(\text{kOe}) = \frac{119n(\text{Fe})}{\sqrt{N}}$$

(N being the total number of nearest neighbors) which was established by Trumpy *et al.*[23] for the crystalline phases.

In Table IV are reported the values of N and n(Fe) in Fe_3Sn, Fe_3Sn_2, and FeSn along with the corresponding hyperfine field measured or calculated by the above formula. If the decrease of N with local impoverishment in iron is attributed to sterical effects (tin atoms are bigger than iron atoms), it may be assumed from Table IV that N is reduced by 1 when n(Fe) is reduced by 2 with maxima of 12 for N and n(Fe). Thus Table IV may be extrapolated as shown in Table V which gives a correspondence between hyperfine field and local environment $(N,n(\text{Fe}))$ of a given iron atom in crystalline or amorphous tin-iron compounds. Then, for each value of x (composition of the alloys) we have determined the probability $P(N,n(\text{Fe}))$ to find the configuration $(N,n(\text{Fe}))$ by stating

$$P(N,n(\text{Fe})) = P(H_i) \ ,$$

$P(H_i)$ being measured on the distribution curves shown in Fig. 3(b) for the particular value of H_i which corresponds to the couple $(N,n(\text{Fe}))$ in Table V. Finally we have calculated the proportion of iron atoms $\mathcal{P}(+m)$ having more than m iron nearest neighbors, that is

$$\mathcal{P}(+m) = \sum_{n(\text{Fe})=m}^{12} P(N,n(\text{Fe})) \ .$$

In Fig. 10 are shown the variations of $\mathcal{P}(+m)$ in function of iron concentration x for m ranging from 3 to 8. We can see that the measured proportion C_H of magnetic iron atoms is roughly parallel to the $\mathcal{P}(+5)$ curve. Thus, even if obtained for a purely gratuitous extrapolation of a phenomenological formula[23] established for a few crystalline tin-iron compounds, the

TABLE IV. Near-neighbor and hyperfine field in crystalline FeSn compounds.

Compounds	N	n(Fe)	H_i (calc) (kOe)	H_i (expt)[a] (kOe)
Fe_3Sn	12	8	276	268
Fe_3Sn_2	11	6	216	216
FeSn	10	4	151	156

[a]Reference 23.

TABLE V. Estimated near-neighbor and hyperfine field in amorphous Fe_xSn_{1-x} alloys.

N	12	12	12	12	12	11	11	10	10	9	9	8	8
n (Fe)	12	11	10	9	8 (Fe_3Sn)	7	6 Fe_3Sn_2	5	4 FeSn	3	2	1	0
H_i (kOe)	414	379	345	320	276	252	216	188	151	119	0[a]	0[a]	0

[a]$H_i < 100$ kOe that is 0 according to fitting procedure (Ref. 21).

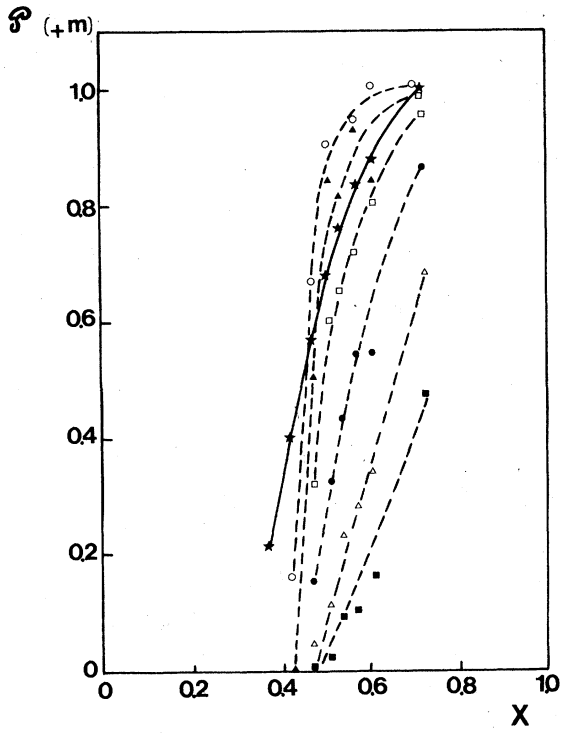

FIG. 10. $\mathcal{P}(+m)$ curves as defined in text with $+m=3(\blacksquare)$, $4(\Delta)$, $5(\bullet)$ $6(\square)$, $7(\blacktriangle)$, or $8(\circ)$ compared to the concentration of iron magnetic atoms $C_H(*)$ (full curve).

results suggest that an iron atom would be magnetic only when it belongs to local configuration including at least five iron atoms in the nearest-neighbor (NN) shell, that is, 5 Fe +5 Sn or 6 Fe +5 Sn or 7+4 Sn or 8 Fe +4 Sn or 9 Fe +3 Sn or 10 Fe +2 Sn or 11 Fe +1 Sn or 12 Fe. The size effect included in this model might be taken into account, along with the diffraction data, in building a structural model for amorphous Fe_xSn_{1-x} alloys and would explain that $C_{tH}(Sn) < C_H(Fe)$ for the alloys of the iron-rich end (Fig. 9) the tin atoms preferably are in "nonmagnetic" configurations.

C. Temperature dependence of the hyperfine field

For the alloys of the iron-rich end ($x > 0.55$) the proportion of magnetic atoms is fairly large [$C_H(x,0) > 0.8$] and the influence of temperature on the hyperfine field can be studied in quite a wide range. Although still controversial, the $H_i(T)$ data are usually interpreted in terms of collective excitations of spin waves, that is

$$\frac{H_i(T)}{H_i(0)} = 1 - B\left(\frac{T}{T_C}\right)^{3/2} - C\left(\frac{T}{T_C}\right)^{5/2},$$

which happens to be valid for amorphous alloys in a T range wider than for crystalline compounds[24] and with a larger value of the B coefficient ($\sim$0.40 compared to $\sim$0.12 in iron or nickel). However, a simple homogeneous Stoner spin-flip model developed in a Landau mean-field formalism which leads to

$$\left(\frac{H_i(T)}{H_i(0)}\right)^2 = 1 - K\left(\frac{T}{T_C}\right)^2$$

is very often a satisfactory alternative interpretation[25] in the intermediate temperature range ($T > 80$ K). Actually the experimental accuracy is hardly good enough to decide definitely which phenomenon is the true one. In some amorphous systems the spin-wave model has been ascertained by a good agreement between the values of the B coefficient obtained from Mössbauer spectroscopy or magnetization measurements and the D spin-wave stiffness constant given by neutron diffraction, especially at very low temperature.[26]

The curve in Fig. 11 has been drawn for our iron-rich amorphous tin-iron alloys and shows a good consistency of the H_i data with a $T^{3/2}$ law up to $T/T_C \sim 0.6$. The B coefficient is the same whatever the alloy composition, very near the values obtained for other amorphous alloys[26] and about 4 times larger than for crystalline iron. The spin-wave stiffness constant D can be estimated from B through the theoretical expression[24]

$$B = \frac{0.612 g \mu_B}{M(0)}\left(\frac{k_B T_C}{4\pi D}\right)^{3/2},$$

in which $M(0)$ is the maximum magnetization per unit volume at $T=0$ K. All these data are reported in Table VI. As expected, D is somewhat smaller in amorphous than in crystalline systems. In the following, a semiquantitative interpretation will be proposed

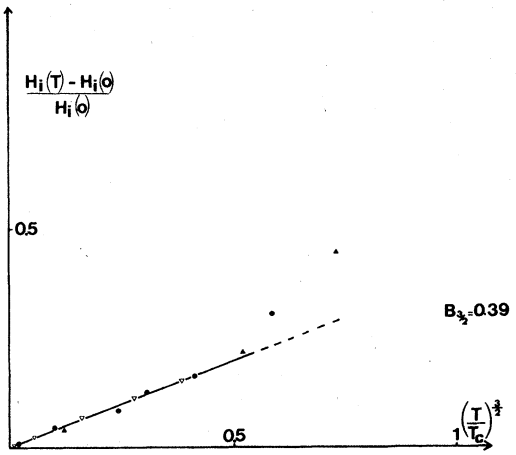

FIG. 11. Reduced mean hyperfine field vs $T^{3/2}$ in Fe_xSn_{1-x} amorphous alloys: $\Delta, x=0.72$; $\bullet, x=0.61$; $\blacktriangle, x=0.57$.

TABLE VI. Comparison of spin-wave parameters B and D for some amorphous alloys and pure iron, and calculated D_0 for amorphous Fe_xSn_{1-x} alloys.

Material		T_C (K)	$M(0)$ (μ_B)	B	D (meV Å^{-2})	D_0 (meV Å^{-2})
Amorphous Fe_xSn_{1-x} alloys	$x=0.72$	550	2.06	0.39	101	154
	$x=0.61$	420	1.80	0.39	90	130
	$x=0.57$	360	1.58	0.39	86	122
Amorphous $(Fe_x, Ni_{1-x})_{75}P_{16}B_6Al_3$[a]	$x=0.65$	576	2.05	0.387	115	
	$x=0.50$	482	2.20	0.455	94	
Crystalline iron[a]		1042	2.22	0.114	281	

[a]Reference 26.

through a calculation of D in a quasicrystalline approximation.[27] The spin-wave dispersion law can be expressed by

$$\omega(\vec{q}) = \mathrm{Re}\left[2S \int J(\vec{r}) g(\vec{r}) [1 - \exp(-i\vec{q}\cdot\vec{r})] \, d^3r\right] ,$$

in which $\vec{q}$ is the wave vector, J the exchange integral at distance $\vec{r}$ in the material, S the spin momentum, and $g(\vec{r})$ the pair-distribution function. In the limit of small q and perfect isotropy, $\omega(\vec{q})$ simplifies into

$$\omega(\vec{q}) = \tfrac{1}{3} S q^2 \int r^2 J(r) P(r) \, dr = Dq^2$$

that is

$$D = \tfrac{1}{3} S \int r^2 J(r) P(r) \, dr$$

with $P(r) = 4\pi r^2 g(r)$ being the probability of finding atoms at distance r from the origin.

Assuming a Gaussian-distribution law for $P(r)$ and a linear dependence of J on the distance r, a straightforward calculation gives

$$D = D_0 \left(1 - 2Z \frac{\Delta r}{r} \frac{\Delta J}{J}\right)$$

with

$$D_0 = \frac{Z J_0 S r_0^2}{3}$$

in which the subscript 0 refers to nearest-neighbor distance (r_0) or exchange integral (J_0), $\Delta r/r$ and $\Delta J/J$ are the relative width of the distribution of r_0 and J_0, Z is the NN iron number and average to the iron concentration x. An estimate of J_0 can be made with the Curie temperature through

$$k_B T_C = \frac{S(S+1)}{3} \int P(r) J(r) \, dr \simeq \frac{S(S+1)}{3} Z J_0 \ .$$

Then D_0 has been calculated with $S = 1$ which gives the values in the last column of Table VI. Using a typical value $\Delta r/r \simeq 0.05$, the theoretical expression of D fits the experimental data (Table VI) if $\Delta J/J \simeq 0.4$.

Looking back at Fig. 11, it is clear that the above

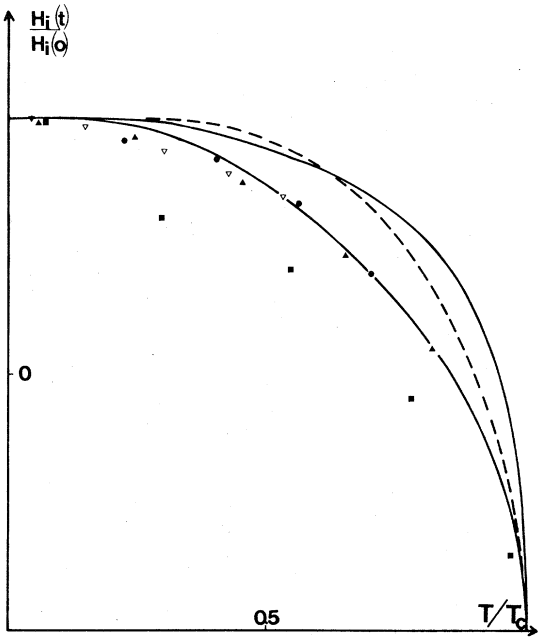

FIG. 12. Temperature dependence of the hyperfine field (reduced coordinate axis) in crystalline iron (dashed line), as calculated through a Brillouin function $S = \frac{1}{2}$ (upper full line) or through the Handrich formula with $\Delta J/J = 0.4$ (lower full line) and in Fe_xSn_{1-x} amorphous alloys: ▽, $x = 0.72$; ▲, $x = 0.61$; ●, $x = 0.57$; ■, $x = 0.53$.

spin-wave interpretation no longer works for intermediate temperatures ($0.6T_C < T < T_C$) where a mean-field theory seems to be more relevant.[25] One mean-field model for disordered alloys is based on a modified Weiss molecular field. This approach has been developed for instance by Handrich[28] and leads to the following expression of the magnetization:

$$\sigma = \frac{M(T)}{M(0)} = \frac{1}{2}\left\{B_S\left[\left(1+\frac{\Delta J}{J}\right)y\right] + B_S\left[\left(1-\frac{\Delta J}{J}\right)y\right]\right\} ,$$

in which B_S is the Brillouin function corresponding to spin S and $y = \sigma(3S/S+1)(T_C/T)$. Assuming that the mean hyperfine field measured in the amorphous Fe_xSn_{1-x} alloys obey the same law, values of $\bar{H}_i(T)/\bar{H}_i(0)$ have been calculated using $S=1$, experimental data for T_C (Table VI or Table III) and $\Delta J/J = 0.4$ as deduced from the spin-wave model at low temperature. As seen in Fig. 12, there is a fairly good agreement between experimental results and calculations for alloys such as $x > 0.55$ and $T_C/T > 0.5$. Contrariwise $H_i(T)$ measured in $Fe_{0.53}Sn_{0.47}$ are quite different of that expected from the mean-field model which may be considered as a fairly good test of the ferromagnetism homogeneity.

D. Properties of the nonmagnetic iron atoms

As pointed out in Sec. IV A, the main features regarding nonmagnetic iron atoms in the Fe_xSn_{1-x} alloys is their contribution to Mössbauer spectra in the form of a quadrupolar doublet with a typical parameter $\Delta\bar{E}_Q(x,T)$ which is a linear function of the mean hyperfine field $\bar{H}_i(x,T)$ arising from the magnetic iron atoms (Fig. 7). Such a linear correlation has been already observed in Fe_xSi_{1-x} amorphous alloys[29] though with two major differences:

(i) The doublet component is obviously asymmetrical for Fe_xSn_{1-x} and was found almost perfectly symmetrical in Fe_xSi_{1-x}.

(ii) The true quadrupolar interaction was somewhat larger in Fe_xSi_{1-x} than in Fe_xSn_{1-x} ($\Delta\bar{E}_Q \simeq 0.5$ mm sec^{-1} and 0.3 mm sec^{-1}, respectively, when $\bar{H}_i = 0$).

Thus, there is an apparent quadrupolar effect which in fact may be due to nonmagnetic iron atoms experiencing a weak magnetic field. This weak magnetic field may in principle have two contributions: one arising from transfer phenomenon through spin polarization of the conduction electrons, and a second being the dipolar field of the magnetic moment $\bar{\mu}$ carried by the magnetic iron atoms.

As previously explained in Sec. IV B, the transferred effect is a short-range one occurring inside "magnetic configurations." Thus, the nonmagnetic atoms which, by definition, are out of magnetic configurations, cannot experience any significant conduction-electron polarization, and the transferred field will be neglected.

The dipolar field can be written

$$\vec{H}^{\text{dip}} = \frac{\mu_0}{4\pi}\sum_{j\neq i}\left(\frac{3\vec{r}_{ij}\cdot\vec{\mu}_j}{r_{ij}^5}\cdot\vec{r}_{ij} - \frac{\vec{\mu}_j}{r_{ij}^3}\right) .$$

Then, the nuclear Hamiltonian of a nonmagnetic iron atom is

$$\mathcal{H} = \mathcal{H}_Q + \mathcal{H}_M$$

with[30]

$$\mathcal{H}_Q = \frac{eQ}{2I(2I-1)}\sum_{\alpha,\beta=1}^{3}\left[\tfrac{1}{2}(I_\alpha I_\beta + I_\beta I_\alpha) - \tfrac{1}{3}I(I+1)\delta\alpha\beta\right]q_{\alpha\beta} ,$$

$$\mathcal{H}_M = -g\mu_N\sum_{\alpha=1}^{3} I_\alpha H_\alpha^{\text{dip}}$$

(in the usual notation for nuclear parameters). The coordinate axis $\vec{0}x_\alpha$ ($\alpha = 1,2,3$) has been taken with $\vec{0}x_3$ parallel to the γ-ray beam (or perpendicular to the sample) and the calculation restricted to the case of uniaxial electric-field gradient with directions randomly distributed in the material. In order to determine the shape of Mössbauer quadrupolar doublet with superposed dipolar field the Hamiltonian $\mathcal{H}$ has been diagonalized; spectra have been calculated with the following numerical values:

$$\tfrac{1}{2}eQq_{33} = 0.3 \text{ mm sec}^{-1} ,$$

$$\frac{\mu_0\langle\mu_j\rangle}{4\pi\langle r^3\rangle} = 10 \text{ kOe} ,$$

$$\Gamma \text{ (linewidth)} = 0.2 \text{ mm sec}^{-1}$$

and the results have been averaged over all the directions of the electric field gradient. The computed spectra shown in Figs. 13(a) and 13(b) correspond to $\vec{\mu}_j$ parallel $(0,0,\mu)$ or perpendicular $(\mu\cos\psi, \mu\sin\psi, 0)$ to the γ-ray beam, respectively. Obviously spectra must have an asymmetrical shape if H_i is perpendicular to the film plane as observed in Fe_xSn_{1-x} amorphous alloys and a relatively more symmetrical profile when H_i is lying in the film plane as previously observed in the Fe-Si amorphous system.[29] Detailed discrepancies between computed and experimental spectra may be ascribed to oversimplifications in the calculations (H_i is not exactly perpendicular to film plane in Fe_xSn_{1-x} and q_{33} should have been described by a distribution). The main conclusion here is that dipolar field, both its intensity and direction, must be taken into account to understand the shape of the nonmagnetic contribution to Mössbauer spectra measured on amorphous alloys.

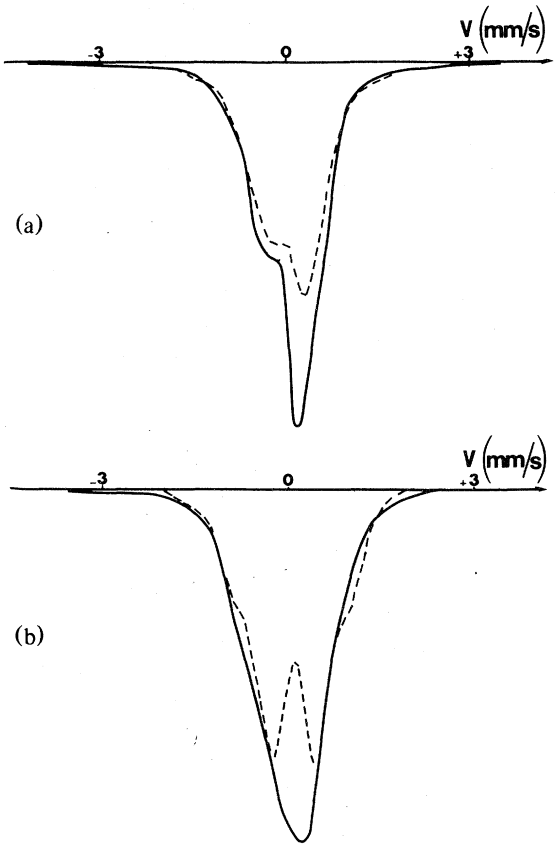

FIG. 13. Nonmagnetic iron-atom contribution to Mössbauer spectra when the magnetization is (a) perpendicular to or (b) lying in the film plane. Calculated patterns (full lines) or experimental spectra from (a) Fe_xSn_{1-x} and (b) Fe_xSi_{1-x} (dashed lines).

V. GENERAL CONCLUSIONS

Structural and magnetic properties of the Fe_xSn_{1-x} amorphous systems have been investigated over quite a wide range of composition. The alloys of the iron-rich end might be described in terms of a dense random packing of hard spheres, but increasing the tin concentration seems to result in the appearance of a more open structure in which the Sn-Sn correlations are very similar to that found in liquid tin and atoms are not hard spheres anymore. Moreover, Mössbauer hyperfine field data suggest that the NN shell of a given iron atom does not have a unique structure and consists of atoms whose total number decrease from about 12 to about 8 if the number of iron atoms in this shell is changed from 12 to 0.

From the magnetic point of view, the only local configurations which contribute to magnetism are those with at least five iron atoms in the NN shell. As a consequence there is an inhomogeneous disappearance of any magnetic order at a critical composition corresponding to about 35% at Fe. Except perhaps very near this critical composition, the alloys of the iron side are ferromagnets with a mixture of magnetic and nonmagnetic atoms.

The hyperfine field and isomer shift distribution measured on the magnetic iron atoms can be ascribed to chemical disorder and are not typical of structural effects. As soon as the iron concentration is larger than about 55 at.%, evidences of homogeneous magnetism behavior are given by the temperature dependence of the mean hyperfine field, which can be interpreted in terms of magnon collective excitations at very low temperature ($T/T_C < 0.6$), and by a mean-field theory at higher temperatures ($0.6 < T/T_C < 1$).

The nonmagnetic atoms are, first, the tin ones which can experience a transferred field when they are included in an "iron magnetic configuration" and, second, some iron atoms subject to a weak dipolar field produced by the magnetic moments of magnetic iron neighbors. The shape of the doublet component, which is the contribution of nonmagnetic iron atoms to Mössbauer spectra, is strongly influenced by magnetic anisotropy.

Detailed studies of the magnetism near the critical composition are now in progress in our laboratory along with careful density measurements and diffraction investigation of similar amorphous systems (TM_xSn_{1-x} with TM = Co, Ni, Mn, Cu) in order to achieve an acceptable description of the short-range order in these materials.

[1]J. F. Sadoc, doctorat d'etat thesis (Orsay, 1976) (unpublished).
[2]Ph. Mangin, G. Marchal, B. Rodmacq, and Chr. Janot, Philos. Mag. 36, 643 (1977).
[3]Ph. Mangin and G. Marchal, Phys. Lett. A 68, 466 (1978).
[4]G. Marchal, Ph. Mangin, M. Piecuch, B. Rodmacq, and Chr. Janot, Mater. Sci. Eng. 36, 11 (1978).
[5]M. Piecuch, G. Marchal, Ph. Mangin, B. Rodmacq, and Chr. Janot, J. Phys. (Paris), Colloq. 35, C4-369 (1974).
[6]O. Massenet, H. Daver, and J. Geneste, J. Phys. (Paris), Colloq. 35, C4-279 (1974).
[7]B. Malaman, doctorat d'etat thesis (Nancy, 1978) (unpublished).
[8]G. Marchal, Ph. Mangin, M. Piecuch, B. Rodmacq, and

Chr. Janot, in *Rapidly Quenched Metals, III,* edited by B. Cantor (The Metal Society, London, 1978), Vol. 2, p. 73.
[9]Ph. Mangin, M. Piecuch, G. Marchal, and Chr. Janot, J. Phys. F 8, 2085 (1978).
[10]G. Marchal, B. Rodmacq, Ph. Mangin, M. Piecuch, and Chr. Janot, in *Proceedings of the International Conference on Mössbauer Effect, Bucharest, 1977,* edited by D. Barb and P. Jariná (Revue Roumaine de Physique, Bucharest, 1977), p. 231.
[11]B. Rodmacq, M. Piecuch, G. Marchal, Ph. Mangin, and Chr. Janot, IEEE Trans. Magn. 14, 841 (1978).
[12]G. Marchal, Ph. Mangin, and Chr. Janot, Philos. Mag. 32, 1007 (1975).
[13]P. K. Leung and J. C. Wright, Philos. Mag. 30, 185 (1974).
[14]P. K. Leung and J. C. Wright, Philos. Mag. 30, 995 (1974).
[15]J. F. Sadoc, J. Dixmier, and A. Guinier, J. Non-Cryst. Solids 12, 46 (1973).
[16]J. E. Enderby, D. M. North, and P. A. Eglestaff, Philos. Mag. 14, 961 (1966).
[17]D. Jovic, I. Padureanŏ, S. Rapeanŏ, and N. Deciu, Rev. Roum. Phys. 21, 585 (1976).
[18]J. F. Sadoc and A. Lienard, *Rapidly Quenched Metals, III,* edited by B. Cantor (The Metal Society, London, 1978), Vol. 2, p. 405.
[19]G. Marchal, Ph. Mangin, M. Piecuch, and Chr. Janot, J. Phys. (Paris), Colloq. 37, C6-763 (1976).
[20]J. Logan and E. Sun, J. Non-Cryst. Solids 20, 285 (1976).
[21]Ph. Mangin, G. Marchal, M. Piecuch, and Chr. Janot, J. Phys. E 9, 1101 (1976).
[22]D. C. Price, J. D. Rush, C. E. Johnson, M. F. Thomas, and P. J. Webster, J. Phys. (Paris), Colloq. 37, C6-617 (1976).
[23]G. Trumpy, E. Both, C. Djega-Mariadassou, and P. Lecocq, Phys. Rev. B 2, 3477 (1970).
[24]C. L. Chien, Phys. Rev. B 18, 1003 (1978).
[25]Ph. Mangin and G. Marchal, J. Appl. Phys. 49, 1709 (1978).
[26]R. J. Birgeneau, J. A. Tarvin, G. Shirane, E. M. Gyorgy, R. C. Sherwood, M. S. Chen, and C. L. Chien, Phys. Rev. B 18, 2192 (1978).
[27]T. Kaneyoshi, Summer School, "Bussei Wakate" at Nozawa, Japan, 1977 (unpublished).
[28]K. Handrich, Phys. Status Solidi 32, K55 (1969).
[29]Ph. Mangin, doctorat d'etat thesis (Nancy, 1977) (unpublished).
[30]Chr. Janot, *L'effet Mössbauer et ses applications* (Masson, Paris, 1972).